Journal of Power Sources 254 (2014) 148–152

Contents lists available at ScienceDirect

Journal of Power Sources

journal homepage: www.elsevier.com/locate/jpowsour

Short communication

Interaction of $La_{0.58}Sr_{0.40}Co_{0.20}Fe_{0.80}O_{3-\delta}$ cathode with volatile Cr in a stack test – Scanning electron microscopy and transmission electron microscopy investigations

Norbert H. Menzler [a,*], Doris Sebold [a], Egbert Wessel [b]

[a] Forschungszentrum Jülich GmbH, Institute of Energy and Climate Research (IEK), IEK-1: Materials Synthesis and Processing, 52425 Jülich, Germany
[b] Forschungszentrum Jülich GmbH, Institute of Energy and Climate Research (IEK), IEK-2: Microstructure and Properties of Materials, 52425 Jülich, Germany

HIGHLIGHTS

- Anode-supported SOFCs with thin-film electrolyte were operated in short stacks for mid-term times.
- Intensive post-test SEM and TEM characterizations were conducted.
- In the GDC barrier layer pores were formed.
- $SrCrO_4$ formation at the border cathode/barrier layer was observed for the first time.
- Degradation rate might be attributed to the detected materials interactions.

ARTICLE INFO

Article history:
Received 28 November 2013
Received in revised form
9 December 2013
Accepted 11 December 2013
Available online 24 December 2013

Keywords:
Solid oxide fuel cell
Thin-film electrolyte
TEM characterization
Degradation

ABSTRACT

Anode-supported solid oxide fuel cells with special thin-film yttria-stabilized zirconia electrolytes made by sol–gel technology were operated in a short stack sequentially for about 1300 h at temperatures of 700 °C and subsequently for 1200 h at 600 °C, respectively. The stack was operated galvanostatically at a constant current density of 500 mA cm^{-2}. After operation, the stack was dismantled and the cells were analyzed with respect to Cr interaction with the LSCF cathode. Chemical analysis revealed typical overall Cr amounts of several tenths μg cm^{-2} cathode area depending on the operation time. SEM cross sections showed less $SrCrO_4$ formation at the typical sites for LSCF (top side of cathode) but there was evidence of chromate formation at the border between the cathode and barrier (electrolyte) layer. This location of foreign phase formation was unexpected. Additional TEM characterizations were therefore conducted. The TEM investigation verified the presence of Cr-containing crystals and revealed pore formation in the barrier layer. The formation of $SrCrO_4$ at this borderline and pore formation were found for the first time after SOFC stack operation.

1. Introduction

To reduce the operation temperature of solid oxide fuel cells, two main development lines are possible for the oxygen-conducting electrolyte layer. One involves the introduction of electrolyte materials with higher oxygen ion conduction compared to classic 8 mol% yttria-stabilized zirconia (8YSZ). Such materials include scandia-stabilized zirconia (ScSZ) or gadolinia-doped ceria (GDC). The latter is particularly suitable for operating temperatures below 650 °C, suppressing electronic conduction which takes place at higher temperatures due to the reduction of Ce^{4+} to Ce^{3+} at low oxygen partial pressures [1]. The other method of overcoming the higher ohmic losses at lower temperatures is to minimize the electrolyte layer thickness. Typical electrolyte thicknesses for anode-supported solid oxide fuel cells (ASCs) are around 10 μm. Such layers are normally applied by conventional ceramic processing like the screen printing of microsized 8YSZ powders. By reducing the electrolyte thickness from 10 μm down to about 1–2 μm, the ohmic resistance of the layer can be reduced by a factor of ~10 at e.g. 650 °C [2] (taking into account the temperature-dependent conductivity and calculations using different electrolyte thicknesses). However, this possibility of reducing the resistance leads to novel problems. If the anode to be coated consists of microsized particles of 8YSZ and NiO, the remaining pores are also

* Corresponding author. Tel.: +49 2461 613059; fax: +49 2461 612455.
E-mail address: n.h.menzler@fz-juelich.de (N.H. Menzler).

0378-7753/$ – see front matter © 2013 Elsevier B.V. All rights reserved.
http://dx.doi.org/10.1016/j.jpowsour.2013.12.066

in the micrometer range. If nanosized structures are then applied, the risk of infiltration and the formation of a dense electrolyte layer that is not smooth are high. Therefore, a graded electrolyte structure was developed and is presented in detail in Ref. [3]. However, Refs. [3] and [4] only discusses basic technological aspects, layer characterizations and single-cell test results. Thus, this publication deals with the next development steps, including testing scaled-up cells (from 50 × 50 mm^2 to stack-relevant sizes of 100 × 100 mm^2) in a stack environment and post-test analysis after mid-term stack operation (~2500 h).

2. Experimental

Typical anode-supported SOFCs provided the basis for developing the thin-film electrolyte cells [5]. In contrast to the classical route, the electrolyte layer applied has special characteristics. After tape casting and pre-sintering (1230 °C), the thick anode support (thickness ~500 μm; NiO Mallinckrodt Baker, Germany, 8YSZ UCM Ceramics, Germany), an anode layer (d ~ 7 μm) composed of 8YSZ (Tosoh Corp., Japan) and NiO were applied by screen printing and subsequent pre-sintering. On this double-layer anode structure, a nanosuspension containing 8YSZ nanosized particles was first applied by spin coating. The nanosuspension coating was repeated once. In between the spin coating steps, the layers were calcined at temperatures of ~500 °C. After the nanosuspension application, a four-layer sol–gel 8YSZ system was applied again by spin coating. The first two layers consisted of a colloidal sol and the latter two of a polymeric sol; details concerning the sols and the coatings can be found in Refs. [3,6]. The complete electrolyte layer was subsequently sintered together with the anode and the substrate at 1400 °C for 5 h. The final electrolyte thickness after sintering was in the range of 1 μm. On top of these half-cells, a ceria–gadolinia barrier layer was applied by physical vapor deposition (PVD, d ~ 200–300 nm) [3,7]. Finally, an LSCF cathode with composition $La_{0.58}Sr_{0.40}Co_{0.20}Fe_{0.80}O_{3-\delta}$ (in-house production by spray drying and calcination) was applied by screen printing. The cathode was sintered at 1040 °C to ensure that it adhered well to the barrier layer and did not destroy the GDC layer, which was coated at lower temperatures during the PVD process (for details concerning the PVD coating and the cathode sintering temperature, please refer to Ref. [8]).

The assembled stack was a four-plane 'F10-design' Jülich stack developed for stationary applications. The interconnects and metal frames were made of Crofer22APU; the sealant was a barium–calcium–aluminum–silicon oxide glass [9], which was transformed into a glass-ceramic during stack sealing. The cells measured 100 × 100 mm^2, each with an active cathode area of approx. 80 cm^2. On the anode side, a nickel mesh was used as the contacting media. On the cathode side, a double layer composed of manganese oxide, which acted as a Cr evaporation protection layer, and then a perovskitic cathode contact layer ('LCC10', in-house production) was coated by wet powder spraying. The stack was sealed at 850 °C for 100 h before the nickel oxide was reduced by slowly enhancing the hydrogen flux [10]. The final operational fuel was hydrogen with 20% water vapor and a fuel utilization of 25%. The stack delivered 0.9 A cm^{-2} at 0.7 V and 650 °C, and the calculated area-specific resistance (ASR) was 170–440 mΩ cm^2. These ASR values are the lowest ever measured for this type of stack design at Jülich. Further operation was carried out for 1300 h at 700 °C followed by a 1200 h period at 600 °C. In both temperature regimes, the average voltage degradation was 2.1–5.7%/1000 h, which is clearly higher than expected compared to 'standard' Jülich ASCs. After mid-term operation, the stack was cooled down and dismantled plane by plane according to internal standards [11]. The cell itself was characterized firstly with respect to Cr incorporation into the cathode with wet chemical methods [12] and secondly with respect to microstructural changes and interdiffusion phenomena with SEM/TEM. For the post-test microstructural investigations, a FEG-SEM Ultra 55 (Zeiss, Germany) and a TEM type Zeiss LIBRA 200Cs INCAEnergy (Zeiss, Germany) were used.

3. Wet chemical analysis of cathode Cr content

The amount of chromium in the cathode was measured by chemically etching the cathode material from the entire cell, dissolving it in acid, and finally detecting the quantitative amount by ICP-OES (inductively coupled plasma-optical impedance spectroscopy); for details please refer to Ref. [13]. The cell cathode area etched was equivalent to 1 cm^2. The measured Cr amounts in the cathode (22–71 μg cm^{-2}) were typical for this design, the cell and contacting materials, the chosen operation conditions and the time, and therefore cannot explain the higher degradation rates.

4. Microstructural results

As stated in the Experimental section, the cells were subjected to post-test analysis with respect to microstructural changes in the electrodes or the electrolyte and with respect to elemental interdiffusions, which may not be suppressed by the thin-film electrolyte.

Fig. 1 shows a SEM cross-sectional image of one cell, and the electrolyte area with the adjacent electrodes at a higher magnification.

No obvious layer deformations, cracking, delamination or anything else are visible at the functional layer area at the higher magnification in Fig. 1. The entire thin films were intact even after the mid-term operation time. No apparent interdiffusions were found, e.g. no Ni on the cathode side and no cathode element on the

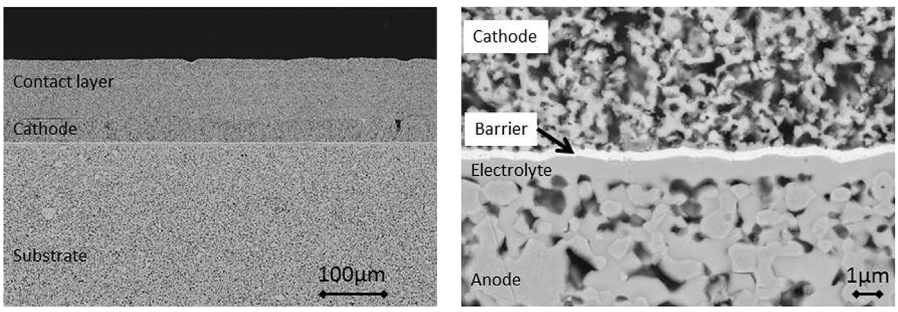

Fig. 1. SEM cross sections of polished surfaces of stack cells operated for ~2500 h at 700/600 °C; left: complete cell overview; right: higher magnification of electrode/electrolyte area.

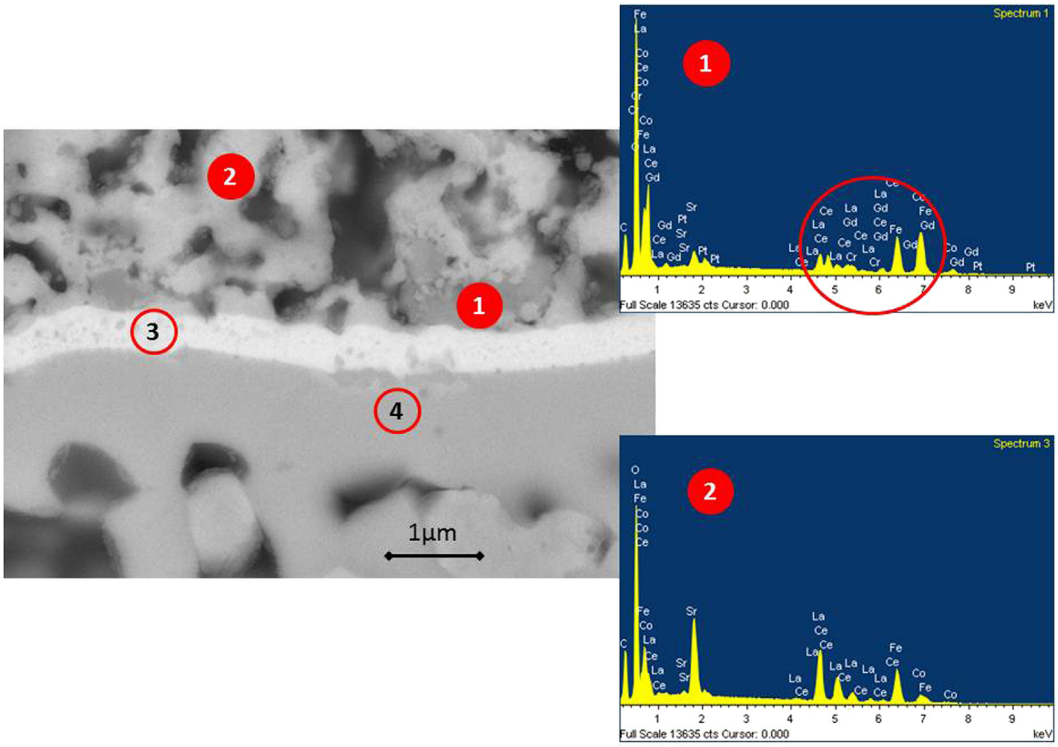

Fig. 2. SEM cross section at high magnification and EDX spectra of points 1 and 2 of the thin-film electrolyte and four markings; no. 1 shows possible phase formation at the cathode/barrier layer; no. 2 is the analyzed area of the cathode bulk material; no. 3 shows color changes in the barrier layer; and no. 4 highlights a second foreign phase formation at the barrier layer/electrolyte.

anode side (proven by EDX point analysis). Furthermore, no $SrZrO_4$ was formed during operation between the barrier layer and the 8YSZ electrolyte. This was due to the complete density of the PVD barrier layer.

However, a closer look at the electrolyte area reveals some changes. Fig. 2 shows four analytical points of interest. At point 2, an EDX spectrum of the bulk cathode can be seen. Only elements from the cathode and some ceria can be detected (Ce due to the large area of excitation of the SEM beam of around 1.5 µm with the cathode). In comparison to point 1, trace amounts of chromium were also found. This was unexpected because according to the literature, the interaction of volatile Cr species with LSCF-type cathodes is only located at the top side of the cathode at its surface, and in stack tests underneath the rims of the interconnects only [14,16]. Our result therefore contradicts the literature. At point 3, color changes within the CGO barrier layer are visible but are difficult to interpret due to the limited magnification of SEM. Finally, at point 4, there may also be some trace foreign phase formation at the electrolyte/barrier border. Again, the area is too

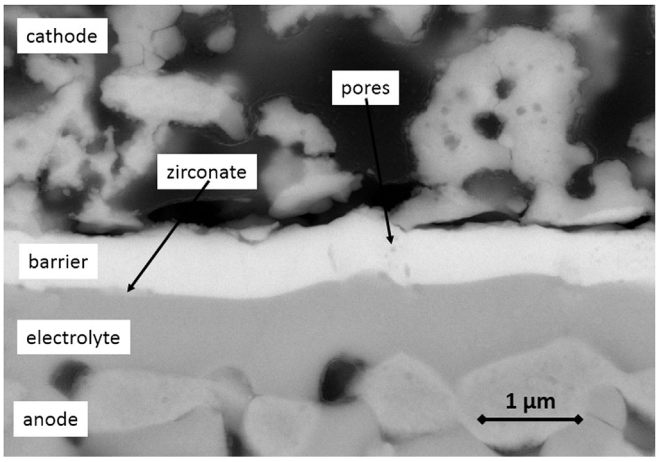

Fig. 3. SEM micrograph of an as-prepared thin-film electrolyte cell.

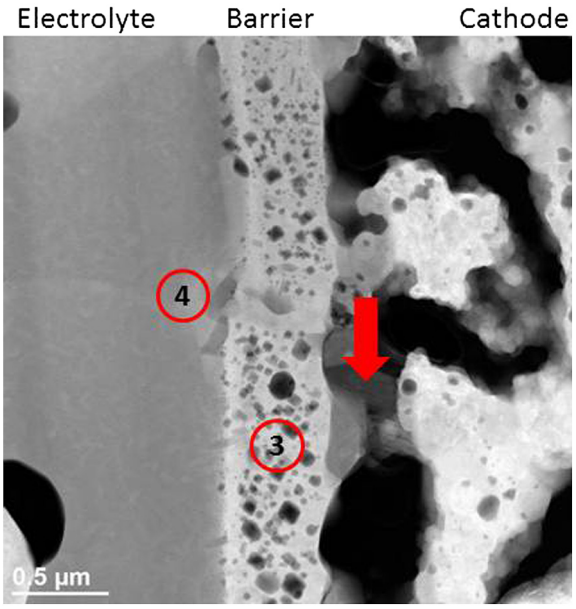

Fig. 4. TEM cross section of the electrolyte/barrier/cathode area; the two numbers mark the same phenomena as in Fig. 2, i.e. no. 3 indicates the changed color in the barrier, and no. 4 the phase formation in the electrolyte; the arrow marks the position of elemental analysis.

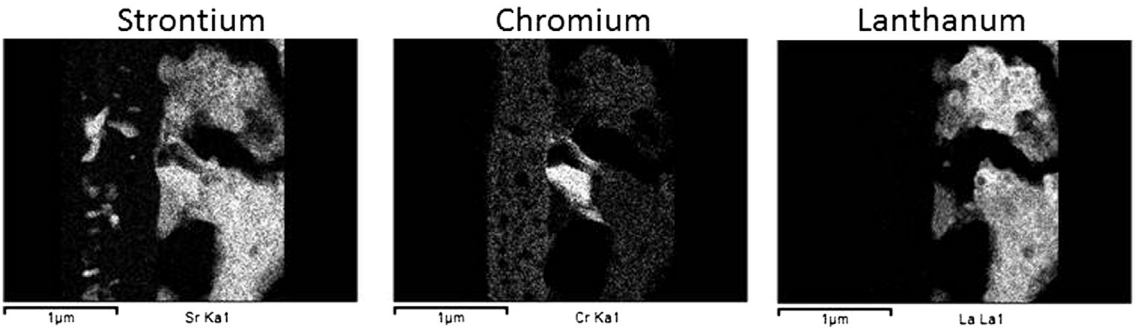

Fig. 5. Elemental analysis of the area of Fig. 3 clearly showing the same distribution for Sr and Cr but not for La.

small to be analyzed by conventional EDX-analysis. It should be noted that $SrCrO_4$ was also found at the top surface of the cathode facing the contact rims of the interconnect, which agrees well with the literature.

For comparison, in Fig. 3 a SEM micrograph of an as-prepared sample is presented. It could be seen that there might be some porosity in the as-prepared buffer layer and that there is some indication for zirconate formation at the border buffer layer/electrolyte. But the amount of pores is less than after stack operation and there is no secondary phase formation visible.

Based on these three findings, none of which can be analyzed properly by means of SEM, additional TEM characterization was carried out. A TEM lamella was prepared by focused ion beam and subsequently characterized. Fig. 4 shows the TEM image. The two interaction phenomena 'phase formation' in the electrolyte and 'color change' in the barrier layer are highlighted. An arrow marks the position of elemental characterization. The color change in the barrier layer indicates the formation of pores, and may be due to Gd diffusion into the electrolyte. Comparable results were found by Uhlenbruck et al. [7], Jordan [8] and Jordan et al. [15], either after GDC application or after mid-term single-cell operation. In the latter, an overall voltage degradation rate of 5.7%/1000 h was calculated after operating a single cell in a ceramic housing at 700 °C and an applied current density of 812 mA cm^{-2} for 1000 h. The calculated degradation rate corresponds well to the rate measured for the stack characterized here. It must be noted that the operating conditions are not completely comparable (with respect to temperature, applied current, operation time and fuel utilization), but the rate does lie in the same region of several percent per thousand hours. None of the cited papers offer an explanation for pore formation, which is still not fully understood.

The elemental analysis of point 4 (foreign phase formation) revealed the formation of $SrZrO_3$. The zirconates are the darker gray regions underneath the barrier, and the light gray structures at the barrier layer/electrolyte represent the Gd interdiffusion. This effect is only found very locally.

Of greater interest was the analysis of the phase marked with an arrow. In Fig. 5, the elemental distribution of Sr, Cr and La is plotted. Sr and La both represent cathode elements and Cr originates from the volatile chromium species from the metal parts within the stack or from the tubing in front of the stack. It can be concluded from the elemental distribution that a Cr–Sr phase (probably $SrCrO_4$) has formed. The analysis showed for the first time that strontium chromate also forms in LSCF cathodes at the border between the cathode and electrolyte (barrier) layers. Future studies will investigate whether this phenomenon is also found in stacks with thick-film electrolytes (~10 µm). This phenomenon has not yet been characterized due to its local distribution and rare formation, or its occurrence only when using a very thin electrolyte (1–1.5 µm 8YSZ + GDC). Another reason for this formation might be the lower sintering temperature of 1040 °C applied to the cathode. Normally, this type of cathode is sintered at 1080 °C when applied to the conventional anode-supported cells with thicker electrolyte layers.

5. Conclusions

Anode-supported solid oxide fuel cells with thin-film electrolytes and diffusion barrier layers were tested in a four-plane short stack environment for mid-term operation times of ~2500 h at low temperatures (700/600 °C). The measured voltage degradation over time was in the range of 2–6%/1000 h, which is too large for this type of cell and stack. Post-test analysis of the cell itself showed fewer interdiffusion phenomena in the functional cell layers; only minor traces of $SrZrO_3$, formed at the electrolyte/barrier layer could be detected. However, intensive SEM and TEM studies revealed two additional changes. One was the formation of numerous nanosized pores within the GDC barrier layer, which may be due to gadolinium diffusing into the electrolyte material. Both materials – 8YSZ and GDC – have very similar crystal structures and the elements can interdiffuse easily and be incorporated into the basic lattice.

The second change was the formation of a foreign phase between the LSCF cathode elements and the volatile Cr species originating from the metallic parts or the tubing. The formed $SrCrO_4$ was located at the top surface of the cathode facing the metallic interconnect rims and at the cathode/barrier (electrolyte) layer. $SrCrO_4$ was found in the latter area for the first time. The chromate formation for the mixed conducting LSCF typically only takes place at the top surface. It has yet to be verified whether the phase formation at the cathode/barrier layer originates from the thin-film electrolyte and thus possibly has different redox potentials compared to thick-film electrolytes, whether this phase formation originates from the lower sintered cathode, or whether it always occurs but in lower concentrations that are randomly distributed and has thus remained undetected until now.

It has yet to be clarified which of the characterized post-test findings – pore formation in the barrier layer, chromate formation at the cathode/barrier layer, or the barrier layer/electrolyte foreign phase formation – is the reason for the higher voltage degradation. It might be speculated that the barrier layer/electrolyte foreign phase formation is not the reason because this phenomenon is typically more pronounced in cells with screen-printed GDCs. The amount of chromate formation at the cathode/barrier layer seems to be relatively small, and may therefore be ruled out as the reason for the enhanced degradation. The pore formation in the barrier layer might enhance the ohmic resistance, and therefore could explain the measured degradation rates. However, this needs to be verified in future.

Acknowledgments

The authors would like to acknowledge the cell manufacturing group and Dr. F. Han at IEK-1 for preparing the cells, stack testing by Prof. L. Blum, Dr. Q. Fang and Mrs. U. Packbier (IEK-3), H. Lippert (ZEA-3) for chemical Cr analysis, and TEM lamella preparation by D. Eßer (IEK-2).

References

[1] J.W. Fergus, J. Power Sources 162 (2006) 30–40 and citations therein.
[2] V.V. Kharton, F.M.B. Marques, A. Atkinson, Solid State Ionics 174 (2004) 135–149.
[3] F. Han, R. Mücke, T. van Gestel, A. Leonide, N.H. Menzler, H.P. Buchkremer, D. Stöver, J. Power Sources 218 (2012) 157–162.
[4] N.H. Menzler, F. Han, D. Sebold, Q. Fang, L. Blum, H.P. Buchkremer, ECS Trans. 57 (1) (2013) 471–480.
[5] L. Blum, L.G.J. de Haart, J. Malzbender, N.H. Menzler, J. Remmel, R. Steinberger-Wilckens, J. Power Sources 241 (2013) 477–485.
[6] T. van Gestel, D. Sebold, H.P. Buchkremer, D. Stöver, J. Eur. Ceram. Soc. 32 (2012) 9–26.
[7] S. Uhlenbruck, N. Jordan, D. Sebold, H.P. Buchkremer, V.A.C. Haanappel, D. Stöver, Thin Solid Films 515 (2007) 4053–4060.
[8] N. Jordán Escalona, Herstellung von Hochtemperatur-Brennstoffzellen über physikalische Gasphasenabscheidung. Schriften des Forschungszentrums Jülich Energy & Environment, vol. 32, 2009, ISBN 978-3-89336-565-4 (available in German only).
[9] S.M. Gross, D. Federmann, J. Remmel, M. Pap, J. Power Sources 196 (17) (2011) 7338–7342.
[10] L.G.J. de Haart, I.C. Vinke, ECS Trans. 35 (1) (2011) 187–194.
[11] N.H. Menzler, P. Batfalsky, in: D. Stolten, B. Emonts (Eds.), Fuel Cells: Science and Engineering Materials, Systems, Processes and Technologies, Wiley-VCH, 2012, ISBN 978-3-527-33012-6, pp. 469–492. Chapter 16.
[12] N.H. Menzler, I. Vinke, H. Lippert, ECS Trans. 25 (2) (2009) 2899–2908.
[13] A. Neumann, N.H. Menzler, P. Batfalsky, S.M. Groß, V. Shemet, F. Tietz, ECS Trans. 35 (1) (2011) 195–206.
[14] E. Konysheva, H. Penkalla, E. Wessel, J. Mertens, U. Seeling, L. Singheiser, K. Hilpert, J. Electrochem. Soc. 153 (2006) A765–A773.
[15] N. Jordan, W. Assenmacher, S. Uhlenbruck, V.A.C. Haanappel, H.P. Buchkremer, D. Stöver, W. Mader, Solid State Ionics 179 (2008) 919–923.
[16] N.H. Menzler, P. Batfalsky, S.M. Groß, V. Shemet, F. Tietz, ECS Trans. 35 (1) (2011) 195–206.